Published in "Journal Of Physics B: Atomic, Molecular And Optical Physics
38(20): 3655–3672, 2005" which should be cited to refer to this work.

Measurement of the elastic and $v = 0 \rightarrow 1$ differential electron–N_2 cross sections over a wide angular range

Michael Allan

Abstract

Absolute differential elastic and vibrational excitation cross sections have been measured for N_2 in the scattering angle ranges starting between 0° and 20° and extending to 180°, at energies between 0.8 and 5 eV. The results agree with many previous measurements, in particular for angles around 90°, but discrepancies were found in some cases for angles close to 0° and 180°. Integral and momentum-transfer cross sections have been derived and compared with previous beam and swarm measurements. The procedures for determining the instrumental response function and for assuring optimal beam overlap over wide ranges of angles and energies are discussed.

1. Introduction

Electron collisions with N_2 are of substantial interest for the ionosphere and plasma processing. N_2 is one of the most studied molecules as far as electron collisions are concerned, both experimentally and theoretically. The work has been reviewed by Schulz [1], Itikawa [2], Zecca *et al* [3] and Brunger and Buckman [4], and a comprehensive crossed-beam and theoretical study has been reported by Sun *et al* [5]. The beam and swarm results have been critically compared by Buckman and Brunger [6] and Robertson *et al* [7]. The elastic and $v = 0 \rightarrow 1$ differential measurements have been extended to 180° using the 'magnetic angle changer' (MAC) by Zubek *et al* [8] and Trantham *et al* [9].

Despite this extended work, open questions remain, in particular, at large scattering angles and for the very small vibrational cross sections below the resonance region. This work completes the existing data at low energies and large scattering angles, regions where the required technologies, in particular the MAC [10, 11], have become available only recently.

Despite the availability of the MAC, measuring differential cross sections at very small and very large angles remains far from trivial. Elaborate strategies are required to assure optimum overlap of the incident beam and the analyser acceptance cone as the electron energies and the scattering angle are changed, and to determine the response function of the instrument for all

the energies and angles required. A few research groups have developed methods to achieve this goal [8, 12], but there are still many inherent uncertainties which are usually apparatus specific. Knowledge of these procedures is essential for the judgement of the reliability of the data and this work therefore serves a secondary purpose; it elaborates on the procedures required to measure differential cross sections at very small and very large angles.

2. Experiment

2.1. The spectrometer

The instrument is a conventional electron spectrometer with two hemispherical electron monochromators and two hemispherical electron analysers [13–15]. The energy resolution was about 14 meV in the energy-loss mode, at a beam current of around 250 pA. The energy of the incident beam was calibrated on the ^{2}S resonance in helium (the more recent energy of 19.365 eV [16] has been used, although it is only insignificantly different from the earlier value of 19.366 eV [17]) and is accurate within $\pm$10 meV. The sample gas was introduced through a 0.25 mm diameter effusive nozzle kept at $\sim$30 °C.

The instrument incorporates the magnetic angle changer invented by Read and co-workers [10, 11], which permits measurements of scattering into the backward hemisphere. The particular form of the MAC realized in Fribourg [18, 19] is made of a few windings of a thin (0.63 mm diameter) copper tubing, cooled by water. This design minimizes the obstruction of the gas flow; the local pumping speed in the collision region is nearly unaffected by the presence of the MAC. This reduces beam attenuation by background gas, is important for absolute measurements which rely on a definite gas flow and improves resolution by reducing the thermal Doppler broadening encountered in scattering by the background gas. The design further simplifies the power supplies since it has only one current loop for both the inner and the outer solenoid. The same computer controls the digital-to-analogue converters determining the incident and scattered electron energies (E_i and E_r) and the MAC current, which is automatically adjusted to provide the desired deflection angle every time E_i and/or E_r are changed. The scattering angle was calibrated by guiding the incident beam into a rotatable Faraday cup and is accurate within $\pm3^\circ$.

It may appear that incorporating the MAC device solves all the problems and the measurement of cross sections over the entire angular range becomes straightforward. A naive use of the device can easily result in errors exceeding a factor of ten, however. The central issues are the following.

- Ascertaining an optimal overlap of the incident beam, the analyser acceptance cone (the 'scattered beam') and the gas beam, when the electron energies E_i and E_r and the scattering angle θ are changed.
- Determining the 'response function' of the instrument as a function of both the electron energies and the scattering angle, and properly correcting the raw data.

These issues will be discussed in more detail here.

2.2. The variation of the instrumental response function with electron energy

The response function for elastic signal is relatively easy to determine, by measuring the He elastic signal as a function of energy and dividing it point by point by the theoretical cross section [20]. In practice, a problem arises because the thermal Doppler broadening and the shift of the elastic peak due to momentum transfer are not negligible in He [21]. The translational excitation is about 9 meV at 20 eV and 135°. The thermal Doppler broadening increases

inherently with scattering angle and electron energy, but depends on scattering angle also for apparative reasons. It is smallest at 90° where the incident and scattered electron beams intersect in a very small volume, about $(0.25\ \mathrm{mm})^3$ in the present instrument, in the front of the nozzle, and the molecules in this effective collision volume move all essentially in one direction. The apparative aspect is worst near 0° and 180° where the incident and scattered electron beams are nearly collinear, probe a large width of the effusive gas beam, with a substantial range of directions of the thermal velocities of the target gas. As a consequence, the elastic peak becomes broader and shifts to higher energy loss ΔE with increasing scattering angle and increasing incident electron energy E_i. The observed width of the He elastic peak in the present experiment was 14 meV at 0.4 eV and 22.5 meV at 20 eV (at $\theta = 135°$), indicating a Doppler broadening of 17.6 meV. This is substantially less than the 45 meV calculated for a stationary sample gas using the expression given by Read [21]. The Doppler broadening is particularly pronounced around 180° where the apparative and inherent effects combine and the width of the elastic peak in helium may reach 50 meV, that is, the Doppler broadening approaches the value of 47.6 meV, calculated for a stationary gas. The consequence is that the area under the elastic or inelastic energy-loss peak must be taken in all measurements, not the peak height. In practice, this can be achieved either by recording the peak signal and correcting it by a smooth function expressing the area/height ratio measured at a few discrete energies, or by measuring many excitation functions at energy losses spanning the range of about (−50 meV; +50 meV), that is, covering the entire elastic peak, and then taking the sum. The former method was used in some earlier work from this laboratory and the latter method is used here.

In theory, the ideal response function should behave as $1/E$, because the ideal incident beam is constant and the analyser acceptance angle should increase with decreasing E_r. The hemispheres operate at a constant pass energy (3 eV in this work), that is, the pencil angle, defined by the size of the pupil apertures, is constant between the hemispheres. The analyser entrance pencil angle then increases as $1/\sqrt{E_\mathrm{r}}$ and the solid entrance angle as $1/E_\mathrm{r}$, with decreasing E_r. This is true provided that the magnification of the analyser entrance lens does not vary significantly with energy. Trajectory calculations [22] indicate that this assumption is approximately true. At low energies, the pencil angle given by this relation exceeds the useful physical dimension of the entrance lens (i.e., the filling factor exceeds about 50%), and this factor becomes limiting. The response then increases slower than $1/E_\mathrm{r}$ with decreasing energy and becomes constant at very low energies. At extremely low energies, the electrons are lost because of stray fields. Similarly, the incident electron beam is ideally constant, but the pencil angle increases with decreasing energy until it reaches the useful diameter of the monochromator exit lens. Below this energy, the beam starts to decrease. At low energies, the incident beam may also lose efficiency because it becomes diffuse or distorted by stray fields.

The response function of the instrument, shown multiplied by E_r to facilitate visual judgement, should thus be approximately constant above a certain energy, above which the spectrometer behaves ideally. Below this energy, the response function still rises with decreasing energy, but slower than $1/E_\mathrm{r}$. At even lower energies, the response function of the analyser alone should be constant and finally drop. The efficiency of the monochromator decreases, making the response function of the entire instrument fall.

Figure 1 illustrates how the response function is derived. The signal generally drops rapidly with increasing energy and some of the curves are shown multiplied by E_r to facilitate visual judgement of the deviation from the ideal $1/E_\mathrm{r}$ behaviour. The signal recorded at $\Delta E = 10$ meV drops less rapidly with E_r than the signal recorded at $\Delta E = 0$ meV, a consequence of the translational excitation and the Doppler broadening. The signal integrated over all ΔE in the range (−50 meV; +50 meV) is shown both as recorded and as multiplied

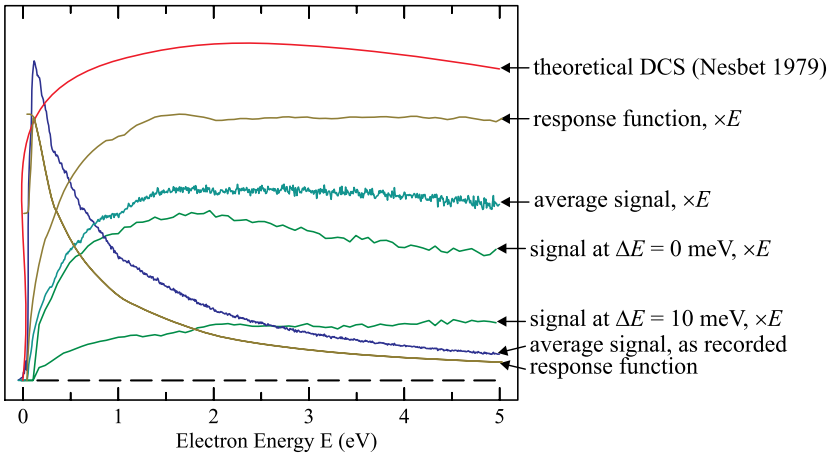

Figure 1. Illustration of how the variation of response function with electron energy is derived. Some of the curves are shown multiplied by the electron energy E to improve the visibility of the deviation from the 'ideal' $1/E$ behaviour. The scattering angle is $\theta = 135°$. The vertical scale is linear and shows the signal intensity, response function and differential He cross section in arbitrary units.

by E_r. The integrated signal divided by the theoretical DCS yields the response function. The curve representing the response function, multiplied by E_r, reveals that the sensitivity of the instrument behaves approximately ideally (as $1/E_r$) at energies $E_r > 1$ eV. At $E_r < 1$ eV, the sensitivity still rises with decreasing E_r, but less rapidly than $1/E_r$, following the expectation outlined above. Finally, at $E_r < 100$ meV, the sensitivity drops rapidly, both because the pencil angle of the incident beam exceeds the useful diameter of the monochromator exit lens and because of stray fields. At an energy range of about 50–100 meV, this drop may still be taken into account for correcting elastic cross sections by making a response function which follows this drop (the dashed line in figure 1). Below 50 meV, such a correction becomes unreliable. The response function for inelastic signal (the full curve in figure 1) is harder to determine. In the past, this response function has been expressed by a product of monochromator and analyser responses [14], the analyser response being determined on the near-threshold ionization continuum of helium. This procedure turns out to be impractical when working at low energies and over large angular ranges and a simplified assumption is made here that the analyser response function is constant below 100 meV. This assumption is justified by the argument about a constant acceptance solid angle outlined above. At 90°, this assumption has been tested independently by using the He ionization continuum to determine the analysis response function.

The He ionization continuum has been used to derive the response function by a number of groups [14, 23, 24]. This method is, however, not suitable for routine response function determination. The underlying assumption of a flat electron distribution is valid only around 90° [23, 25] and the method is consequently not applicable at small and large scattering angles. Furthermore, the He ionization continuum is weak and long accumulation is required. The incident energy is well above the ionization energy during this acquisition, and this appears to change the charging of the surfaces around the collision region and changes the behaviour of the instrument at low energies. This method of determining the response function thus detrimentally affects the performance at low energies, the property which it tries to determine. To provide an independent check of the response function, He inelastic cross sections were recorded from time to time during the present work and compared with earlier data [14, 18].

Another useful test of consistency is recording briefly the vibrationally inelastic cross sections in CO_2 and comparing to earlier results [13, 26].

An important aspect of the measurement is 'tuning' of the instrument, that is determining a set of focusing and x, y-deflection voltages of the monochromator exit and analyser entrance lens insuring optimal focusing and beam overlap over a range of electron energies and scattering angles. This is done by optimizing elastic and inelastic signals in helium, sometimes also in CO_2 and N_2, for a number of discrete electron energies and scattering angles (the 'pivotal points'). The computer then automatically interpolates these parameters between the pivotal points during acquisition. The tuning is the most critical and time-consuming step of the measurements and there are several aspects to which attention has to be paid. One is that it is relatively easy to optimize beam overlap at several energies by optimizing the elastic signal, but much harder to assure that the beam–nozzle distance remains constant for all these energies. This is an imperative condition because without it the beam overlap will be non-optimal for inelastic scattering and the inelastic signal intensity will be seriously wrong (too low) despite the fact that the elastic response function has been optimized and looks correct. The procedure used here is to optimize the inelastic signal in helium (one of the four $n = 2$ states, whichever gives the strongest signal at the energy and the scattering angle in question) for a range of residual energies from threshold to about 5 eV above. While doing so, the incident energy is in the range of ∼20–25 eV, it changes by only a small percentage and the incident beam–nozzle distance may be assumed to remain constant. The analyser acceptance cone is thus tuned for a constant distance to the nozzle. Constant incident beam–nozzle distance at low energies is then achieved by tuning the monochromator exit lens for optimum match with the analyser on elastic scattering in the 0–5 eV range. Parameters giving maximum signal are always sought during the tuning—signal is never reduced intentionally to obtain the desired shape of the response function! Elastic signal cannot be measured below $\theta = 10^\circ$ and inelastic signal (for example, $v = 0 \rightarrow 1$ in N_2 or electronic excitation in He) must be used for tuning at 0°.

The data in figure 1 have small residual dips at certain energies, caused by remaining imperfections in the match of the incident and scattered beams. Such imperfections can generally be further reduced by a prolonged 'tuning'.

2.3. The response function's dependence on scattering angle

As outlined above, the major challenge is keeping optimal beam overlap both for varying angles and for varying energies. The deflector and focusing voltages are optimized for a number of pivotal angles and voltages, and the instrument interpolates between these voltages as energies and angles are scanned. Experience shows that the present instrument cannot be optimized over the entire angular range with a single set of tuning voltages because of what could be called a 'memory effect'. When the instrument is tuned at, as an example, $\theta = 45^\circ$, then moved to say $\theta = 135^\circ$, optimized there, and then returned back to $\theta = 45^\circ$, it 'remembers' that it was 'parked' at $\theta = 135^\circ$ and the optimization at $\theta = 45^\circ$ is no longer valid. It appears that the elastically scattered electrons 'splash' around the collision region and create surface potentials which depend on the position of the analyser. The effect of these potentials can be compensated by suitable deflector voltages, but when the instrument is parked at a different angle for some time, the surface potentials change, and the previously determined deflector voltages are no longer applicable.

This problem is circumvented here by repetitively scanning the scattering angles over only a part of the angular range and merging the partial angular measurements together at the end. The entire angular range has been divided into three overlapping angular fragments. The analyser was placed at the angles of $\theta = 45^\circ, 90^\circ$ and 135°, and the angle was repetitively

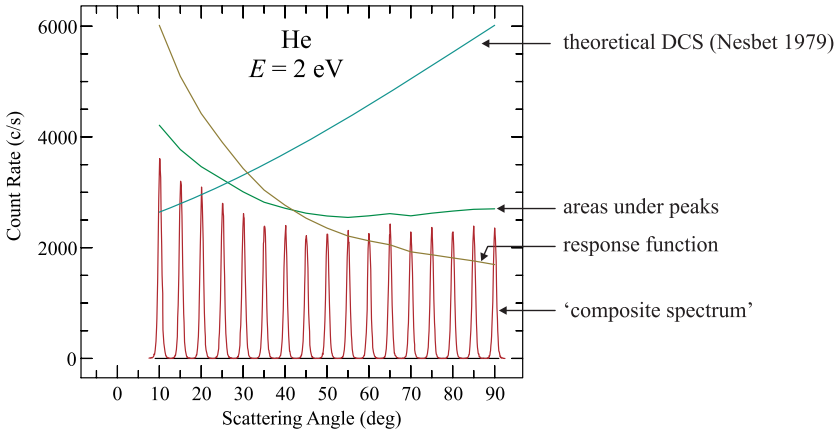

Figure 2. Illustration of how the angular response function is generated.

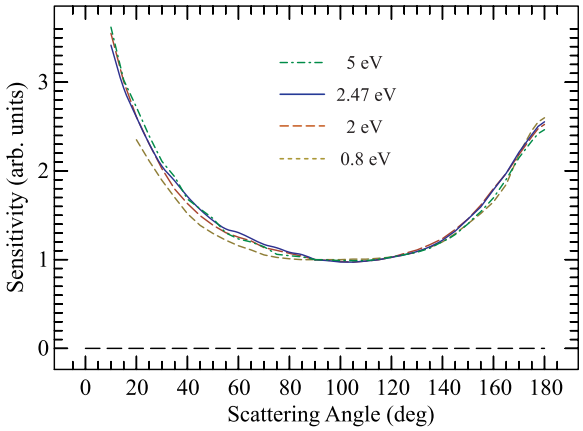

Figure 3. The angular response functions for the energies given, normalized arbitrarily to 1 at 90°. Only the functions centred around 45° and 135° are shown, those centred around 90° were omitted to avoid congestion of lines.

magnetically scanned in a range ±45° around the mechanical analyser position. The steps involved in determining the response function's dependence on scattering angle are illustrated in figure 2. A series of short energy-loss spectra around the elastic peak, one at each angle, is recorded. The series is labelled 'composite spectrum' in figure 2. The areas under the elastic peaks are then taken and divided by the theoretical DCS to yield the response function. The instrument cannot distinguish between nearly forward scattered and unscattered electrons, resulting in a large background for elastic spectra at a small angle. The lowest attainable angle is about 15° at 1 eV and slightly below 10° at higher energies.

The resulting response functions for several electron energies are shown in figure 3. Qualitatively, they behave in the expected way, they increase below and above 90° as the spatial overlap of the incident and scattered beams increases. The function levels off near 180° because the overlap with the target gas beam becomes limiting. The response function is not entirely symmetric around 90° and the reason for this is not quite clear. It could be the consequence of the collision volume moving slightly closer to the nozzle at small scattering angles because of slightly changing stray fields as the scattering angle is decreased. The shape

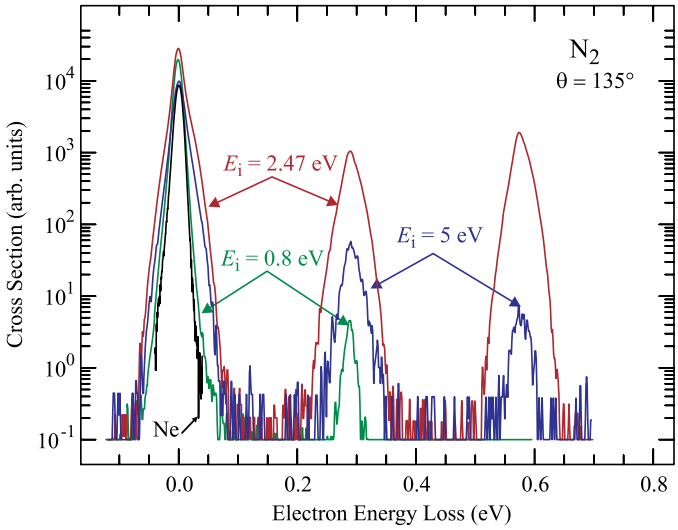

Figure 4. Electron energy-loss spectra used to determine the absolute inelastic cross sections. The elastic peak recorded with neon, representative of the apparatus profile, is also shown.

of the response functions shown in figure 3 is reasonably independent of electron energy, indicating that the beams remain well focussed in this energy range and the response functions determined on elastic scattering may also be used to correct inelastic signal, provided that the instrument has been properly tuned as described above (particular attention being paid to constant beam–nozzle distance with varying energies).

The response function cannot be measured in this way below 10° (below 20° at 0.8 eV), but it is justified to extend it assuming that it has the same (mirror) shape near 0° and 180°. It will be shown below that this assumption leads to a $v = 0 \rightarrow 1$ cross section with the expected d_π shape [27], so that it appears safe to determine the response function below 10° on N_2 in the future (the N_2 standard being applicable only in the 2–3 eV range, however).

2.4. Normalization to absolute values

Absolute values of the elastic cross sections were determined at 45°, 90° and 135° and the incident energies of 0.8, 1.989, 2.47 and 5.0 eV by comparison with the theoretical helium elastic cross section [20], using the relative flow method, described in detail by Nickel *et al* [28]. They are accurate within about ±15%. Energy-loss spectra were then recorded at these four incident energies, corrected for the instrumental response function determined as described in section 2.2. Examples of the energy-loss spectra are shown in figure 4. Absolute inelastic cross sections were determined from the absolute elastic values and the integrals under the elastic and inelastic energy-loss bands. Both the elastic and the $v = 0 \rightarrow 1$ inelastic peaks are barely broader than the elastic peak of Ne at $E_i = 0.8$ eV, but substantially rotationally broadened with $E_i = 1.988$ and 2.47 eV. This confirms the well-known fact that rotational excitation is weak below the $^2\Pi_g$ resonance and strong in the resonance region. The present cross sections were derived from the areas under the peaks and are thus summed over all rotational transitions. The inelastic cross sections are accurate within about ±20%. The absolute values are cited in table 1.

The three overlapping sections of the angular distribution are then joined together as shown in figure 5. Each of the three sections is normalized to an absolute value separately, providing

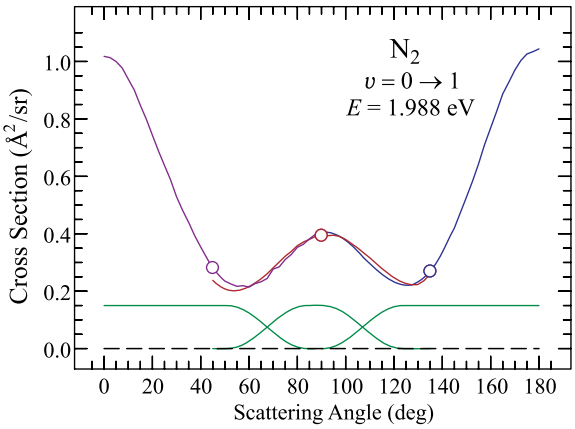

Figure 5. The three segments of the angular distribution spectrum. The circles indicate the three independent determinations of the absolute value. The curves at the bottom show the weighting factors used to join the segments.

Table 1. Summary of the present absolute cross sections. The differential cross sections ($\partial\sigma/\partial\Omega$) are in Å^2 sr^{-1} and the integral (σ_i) and momentum-transfer (σ_m) cross sections are in Å^2.

	$\partial\sigma/\partial\Omega$				
E (eV)	45°	90°	135°	σ_i	σ_m
		$v = 0 \rightarrow 0$			
0.8	0.411	0.849	0.835	8.9	10.2
1.988	1.174	1.284	1.075		
2.47	2.210	1.164	1.676	22.9	21.9
5.0	1.424	0.640	0.652	11.0	9.19
		$v = 0 \rightarrow 1$			
0.8	0.000 49	0.000 26	0.000 23	0.0045	0.0036
1.988	0.279	0.400	0.264	4.64	4.65
2.47	0.097	0.147	0.098		
5.0	0.005 2	0.005 5	0.004 8	0.075	0.073
		$v = 0 \rightarrow 2$			
1.988	0.149	0.205	0.140		
2.47	0.174	0.241	0.171		
5.0	0.000 46	0.000 82	0.000 53		

a desirable degree of redundancy and cross-check. Small adjustments of the absolute values are sometimes necessary before joining the sections together. A smooth transition between the sections is achieved by gradually decreasing the contribution of one section and simultaneously increasing the contribution of the next section, using the 'weighting factors' shown in figure 5. The weighting factors behave as $\cos^2$ and $\sin^2$ in the transition angular range, so that their sum is always equal to 1.

3. Results and discussion

Figures 6–10 show the rotationally summed elastic cross sections at five representative scattering angles, obtained by summing excitation functions recorded at energy losses between

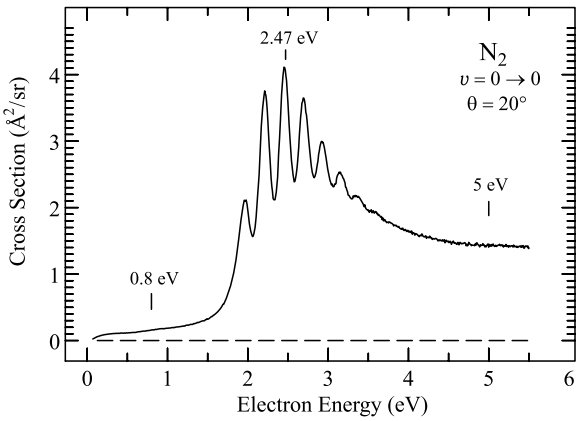

Figure 6. The rotationally summed elastic cross section at 20°. The three energies at which the angular distributions have been measured are indicated.

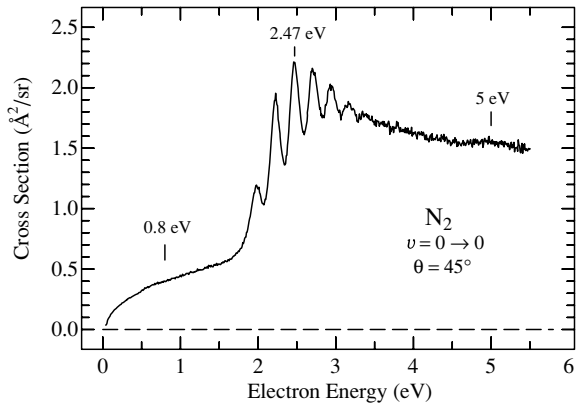

Figure 7. The rotationally summed elastic cross section at 45°.

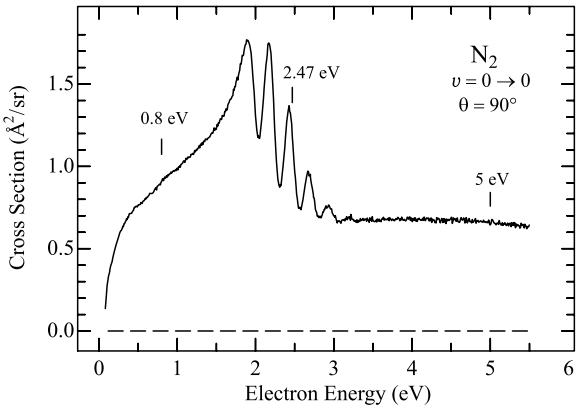

Figure 8. The rotationally summed elastic cross section at 90°.

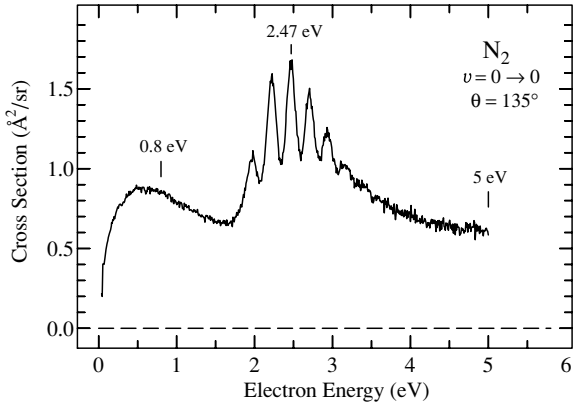

Figure 9. The rotationally summed elastic cross section at 135°.

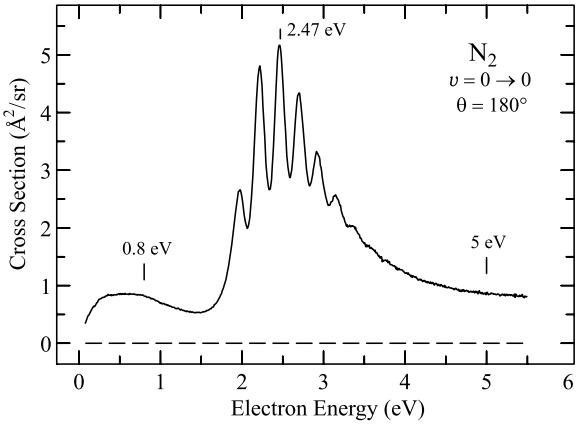

Figure 10. The rotationally summed elastic cross section at 180°.

−50 meV and +50 meV (at 2 meV intervals), correcting the result for the response function determined as described in section 2.2 and normalizing them to agree well with the absolute values determined at the discrete energies of 0.8, 1.988, 2.47 and 5.0 eV. A certain compromise must be made while normalizing because the excitation functions do not agree with the discrete measurements perfectly at all four points.

The figures illustrate the well-known fact that the shape of the elastic cross section depends substantially on scattering angle, because of the coherent superposition of the direct and resonant contributions. As pointed out by Shi *et al* [29] and Sun *et al* [5], this leads to variations of the positions of the resonant peaks with scattering angle and complicates the comparison of angular distributions obtained by various experiments and by theory. Shi *et al* measured their angular dependence around 2.2 eV, with the exact energy adjusted to stay on the peak, but most other authors and the present work measure the angular distributions at fixed electron energies. The peak positions measured in the present work are given in table 2.

The peak positions found here agree well with those of Sun *et al* [5], who reported the third peak in the elastic cross section at 2.46 eV and the first peak in the $v = 0 \rightarrow 1$ cross section at 1.98 eV (at 60°). The peaks are wide and have a relatively flat top, making determination

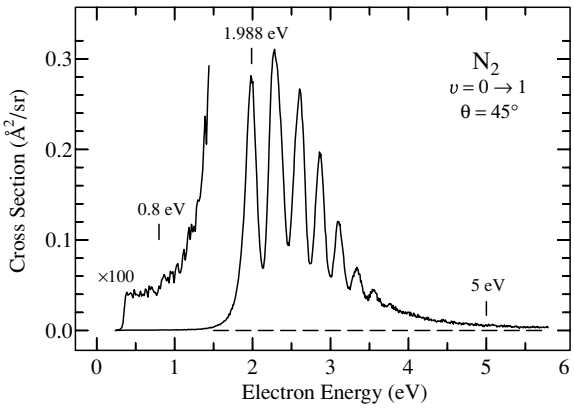

Figure 11. The rotationally summed $v = 0 \rightarrow 1$ cross section at 45°. The three energies at which the angular distributions have been measured are indicated.

Table 2. Measured positions of the third peak in the elastic cross sections and the first peak in the $v = 0 \rightarrow 1$ cross sections (in eV, within ±0.015 eV).

	Scattering angle				
	20°	45°	90°	135°	180°
Elastic	2.455	2.465	2.430	2.467	2.458
$v = 0 \rightarrow 1$	1.980	1.985	1.988	1.988	1.990

of the peak position better than about ±15 meV, difficult even with precise energy scale calibration. The peak position in the $v = 0 \rightarrow 1$ cross section is constant within the accuracy of the experiment. The position of the peak in the elastic cross section varies, but a significant deviation is found only around 90°, where the third peak is 40 meV below the value of 2.47 eV at which the present angular distributions have been measured. The substantial width of the boomerang structures has the consequence that the cross section values do not appreciably change with electron energy for deviations of up to about ±20 meV from the peak, the only substantial difference in the present work being around 2.47 eV and 90°. Reference to the data in figure 8 reveals that the elastic cross section at 2.47 eV would be about 13% larger around 90° if it were measured on peak instead at the constant energy of 2.47 eV used in figure 15.

Figures 11–13 show the rotationally summed $v = 0 \rightarrow 1$ cross sections. The curves have, within experimental error, the same shapes in the resonance region (about 1.7–4 eV). The two curves measured at 45° and 135° also have the same magnitude and are consequently compatible with an angular distribution symmetrical around 90°. The curves are distinctly different below the resonance, in the 0.5–1.5 eV range. The difference appears to be real and is reflected also in the angularly resolved data at 0.5 and 1 eV of Sohn *et al* [30], who found the ratio of the 1 eV/0.5 eV data to be 3.6 at 45° and 2.3 at 135°.

Figures 14–19 show the rotationally summed angular distributions obtained at the energies marked in figures 6–13. The data are compared with selected earlier experimental work and with the theoretical results of Morrison and co-workers [5, 31, 32]. They use the body-frame vibrational close-coupling theory described by Sun *et al* [5]. Correlation-polarization effects were included using either the 'better-than-adiabatic-dipole' (BTAD)

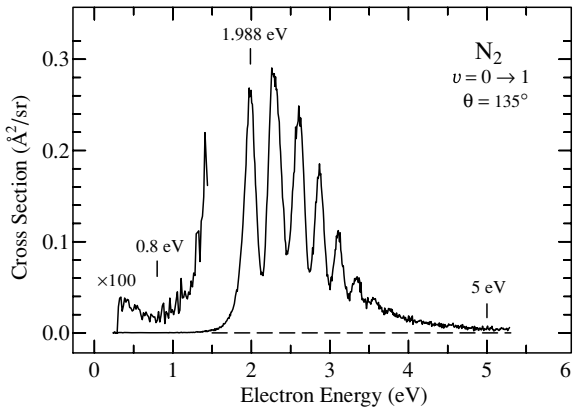

Figure 12. The rotationally summed $\upsilon = 0 \rightarrow 1$ cross section at 135°.

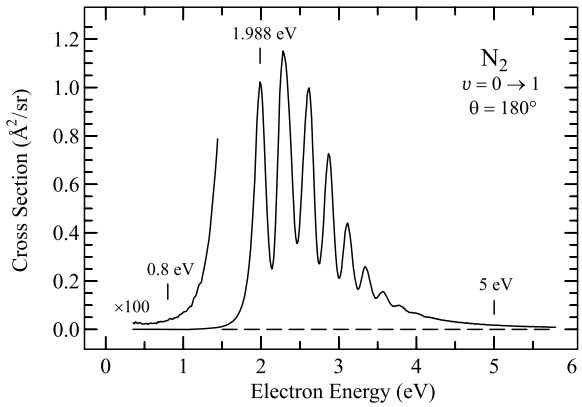

Figure 13. The rotationally summed $\upsilon = 0 \rightarrow 1$ cross section at 180°.

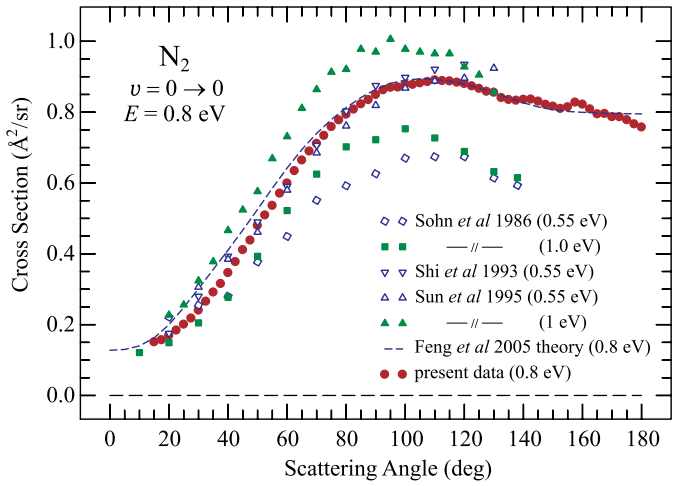

Figure 14. The rotationally summed elastic cross section at $E = 0.8$ eV. The experimental results of Sohn *et al* [30], Shi *et al* [29], Sun *et al* [5] (not at the same energies) and the theoretical results of Feng *et al* [31, 32] (DSG model) are shown for comparison.

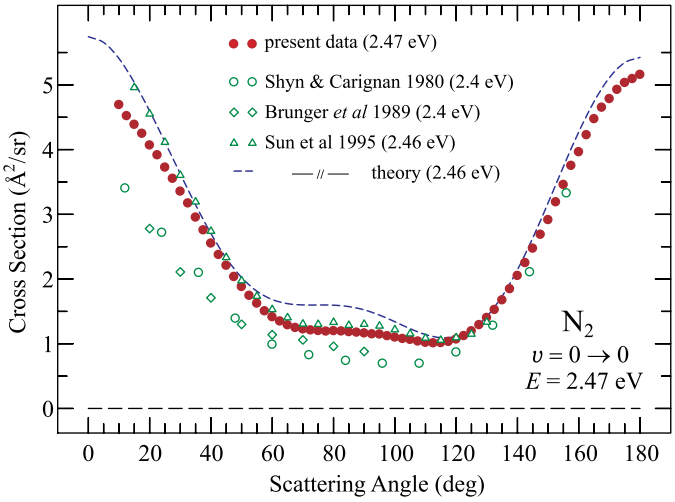

Figure 15. The rotationally summed elastic cross section at $E = 2.47$ eV. The results of Shyn and Carignan [34], Brunger *et al* [24] and Sun *et al* [5] (at nearly the same energies) are shown for comparison.

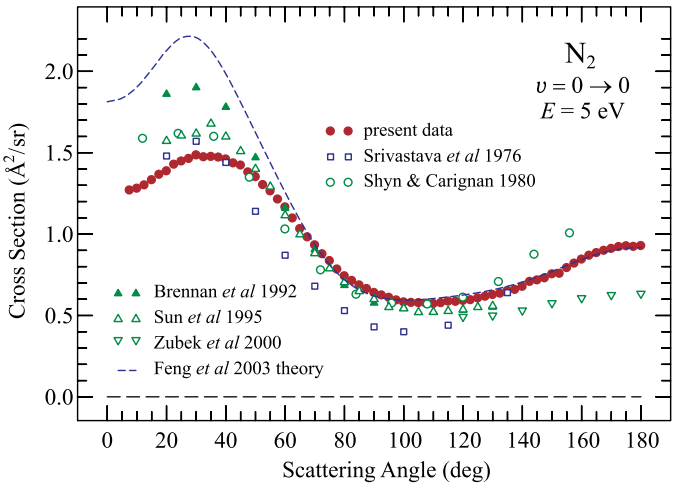

Figure 16. The rotationally summed elastic cross section at $E = 5$ eV. The results of Srivastava *et al* [35], Shyn and Carignan [34], Brennan *et al* [36], Sun *et al* [5], Zubek *et al* [8] and the theoretical results of Feng *et al* [31, 32] (DSC model) are shown for comparison.

potential [33] or the 'distributed spherical Gaussian' (DSG) model [31]. Both models have been extensively compared with experiment and with each other [5, 31]. No published theoretical data were available at 0.8 eV but were kindly provided by Feng *et al* [32] as a private communication.

The data in figure 14 are compared to earlier experimental data at 0.55 and 1.0 eV because no data at 0.8 eV were available in the literature. The cross section increases monotonically in this energy range and the present values should be between those at 0.55 and 1.0 eV. They are slightly higher than those of Sohn *et al* [30] and agree well with those of Shi *et al* [29] and

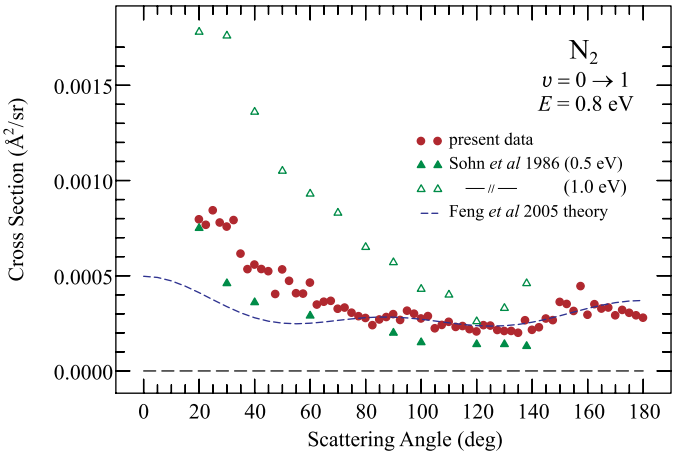

Figure 17. The rotationally summed $\upsilon = 0 \rightarrow 1$ cross section at $E = 0.8$ eV. The experimental data at nearby energies of Sohn *et al* [30] and the theoretical results of Feng *et al* [31, 32] (DSG model) are shown for comparison.

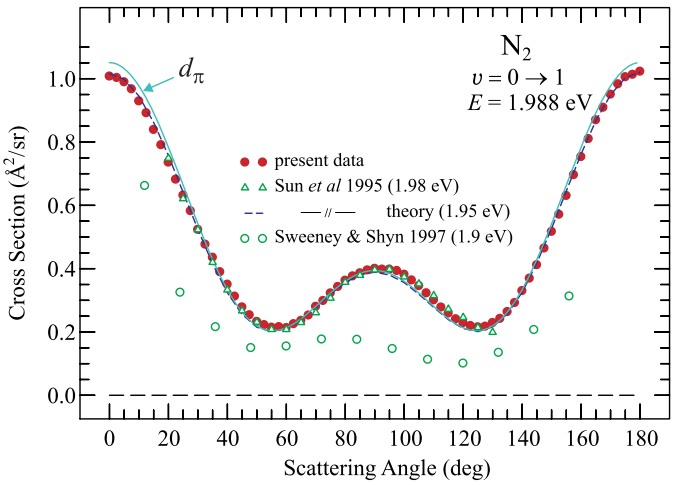

Figure 18. The rotationally summed $\upsilon = 0 \rightarrow 1$ cross section at $E = 1.988$ eV. The results of Sun *et al* [5], Sweeney and Shyn [37] and the d_π wave distribution, normalized to the experiment at 90°, are shown for comparison.

Sun *et al* [5]. The present data are in a very good agreement with the DSG theoretical results of Feng *et al* [32],

The elastic data at 2.47 eV in figure 15 are in an excellent agreement with those of Sun *et al* [5], except for a small difference below 30°. The elastic data at 5 eV in figure 16 are in an excellent agreement with all other results in the intermediate angle range, about 50–120°. Larger differences are found at the more extreme angles. The data of Brennan *et al* are slightly larger below 40°. The theory of Feng *et al* [31, 32] is larger than all experiments at small angles, but agrees very well with the present experiment at the intermediate and backward angles. The data of Shyn and Carignan [34] are larger and those of Zubek *et al* [8] are smaller than the present data at large angles.

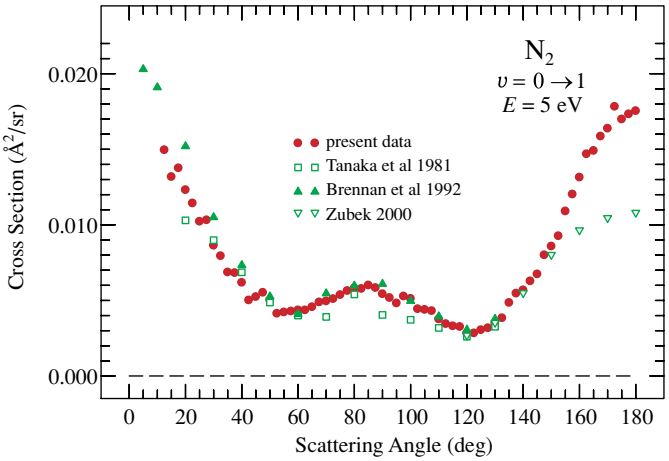

Figure 19. The rotationally summed $v = 0 \rightarrow 1$ cross section at $E = 5$ eV. The results of Tanaka *et al* [38], Brennan *et al* [36] and Zubek *et al* [8] are shown for comparison.

The $v = 0 \rightarrow 1$ data in figure 17 are in a good agreement with those of Sohn *et al* [30] when it is taken into account that the cross section is relatively flat in the 0.5–0.8 eV range and rises steeper above 0.8 eV, as indicated by theory and swarm data (figure 8 of Robertson *et al* [7]). The $v = 0 \rightarrow 1$ cross section in the resonance region (figure 18) is in an excellent agreement with both the theory and the experiment of Sun *et al* [5]. It also agrees very well with a pure d_π distribution, given by the expression $1 - 3\cos^2\theta + \frac{14}{3}\cos^4\theta$ [27], although this comparison must be done with caution, since $\Delta J > 0$ transitions have different angular distributions [39].

The $v = 0 \rightarrow 1$ cross section at 5 eV (figure 19) is in a very good agreement with the earlier data shown, except that the data of Zubek *et al* [8] are lower above 160°. The present data are largely symmetric around 90° and indicate that the excitation is dominated by the $^2\Pi_g$ resonance even at 5 eV.

The integral and momentum-transfer cross sections derived from the present angular distributions are compared to earlier data in table 3. The $v = 0 \rightarrow 1$ cross section in the resonance region did not require any extrapolation, the remaining data required an extrapolation over a narrow angular range around 0°. It was done 'visually' using the shape of the theoretical data as a guide. The shape of the extrapolated data is not critical, the angular range where it is necessary is narrow and the weight in the integration is low.

Buckman and Brunger [6] discussed in great detail the relation of swarm and beam data. In their figure 8, they show an overview of the momentum-transfer cross sections in N_2 below 1.5 eV and some of the data are included in table 3 for comparison. A very similar data compilation was given by Robertson *et al* [7] in their figure 6. Some of the data had to be interpolated between neighbouring energies, which can be done reliably because the cross section is nearly constant in the range in question.

Momentum-transfer cross sections have been investigated by Robertson *et al* [7]. The theoretical cross section of Robertson *et al* [7] given in table 1 are, in the resonance region, not at exactly the energies of the measurements, but at the closest peak (examples: the theoretical integral elastic cross section at 2.484 eV is compared to the measurement at 2.47 eV, the theoretical integral $v = 0 \rightarrow 1$ cross section at 1.95 eV is compared to the measurement at 1.988 eV).

Table 3. Integral and momentum-transfer cross sections (in Å^2). The theoretical values in the resonance region are taken not exactly at the given experimental energy but at the nearest peak in the cross section as a function of energy.

	Integral			Momentum transfer		
E (eV)	Present	Other experiments	Theory[a]	Present	Other experiments	Theory[a]
			$v = 0 \rightarrow 0$			
0.8	8.9	(9.5)[b]	9.54, 9.12[c]	10.2	11.0[d], 9.9[e], 10.6[b], 10.0[f], 10.0[g]	10.34, 10.29[c]
2.47	22.9	24.5[h], 30.6[i]	26.7, 26.62[c]	21.9	23.2[h]	24.95
5.0	11.0	10.9[b], 11.3[j]	13.1, 12.2[c]	9.19	8.64[b]	9.52, 9.67[c]
			$v = 0 \rightarrow 1$			
0.8	0.0045	0.0052[d], 0.0058[k]	0.0017, 0.0035[c]	0.0036		0.0021, 0.0034[c]
1.988	4.64	4.56[b(*)], 2.33[l]	4.53, 4.55[c]	4.65		4.53
5.0	0.075	0.061[m], 0.080[j], 0.077[n]	0.146, 0.129[c]	0.073	0.053[m]	0.147, 0.139[c]

[a] Robertson *et al* [7] and Feng *et al* [31, 32] (swarm data and theory, BTAD model).
[b] Sun *et al* [5] (beam data). The value in parenthesis has been interpolated between the values at 0.55 eV (9.12 Å^2) and 1.0 eV (9.84 Å^2). The value with an asterisk has been given in [7].
[c] Feng *et al* [31, 32] (theory, DSG model).
[d] Haddad [40] (swarm data).
[e] Phelps and Pitchford [41] (swarm data), as cited in [6].
[f] Sun *et al* [5] (time-of-flight data), see also Buckman and Brunger [6].
[g] Ramanan and Freeman [42] (swarm data).
[h] Trantham *et al* [9] (beam data, with magnetic angle changer).
[i] Jung *et al* [39] (beam data).
[j] Brennan *et al* [36] (beam data).
[k] Sohn *et al* [30] (beam data), interpolated between 0.5 eV (0.0048) and 1.0 eV (0.0093), using the theoretical shape of Robertson *et al* [7].
[l] Sweeney and Shyn [37] (beam data).
[m] Tanaka *et al* [38] (beam data).
[n] Zubek *et al* [8] (beam data, with magnetic angle changer).

Sohn *et al* [30] derived integral $v = 0 \rightarrow 1$ cross sections at 0.5, 1.0 and 1.5 eV from their beam data. They obtained the values 0.0048 and 0.0093 Å^2 at 0.5 and 1.0 eV, respectively. Taking into account that the cross section is relatively flat between 0.5 and 0.8 V and starts to rise steeply after that, their data agree quite well with the present results.

4. Conclusions

This work is concerned with extending the angular range of measured differential cross sections and application of this technique to elastic and $v = 0 \rightarrow 1$ cross sections in N_2 up to 5 eV. The invention of the magnetic angle changer was a decisive step in this respect. But in addition to constructing the MAC device, it is necessary to develop elaborate strategies to assure optimum overlap of the incident beam and the analyser acceptance cone as the electron energies and the scattering angle are changed, and to determine the response function of the instrument for all the energies and angles required.

This work describes in more detail a set of such procedures. These efforts are hampered by the notorious drifts of the electron spectrometers, felt particularly at low energies and at small scattering angles, and caused by the changes of the surface conditions of the electron optics in the presence of the sample gas and upon bombardment by electrons and possibly

ions. A further complication is the 'memory effects' whereby the surface potentials vary in function of at what scattering angle and electron energy the instrument was 'parked' prior to a given measurement. Finally, the thermal Doppler broadening, the rotational broadening and (for the He standard) the translational excitation have to be taken into account properly.

The set of strategies described here is not perfect in the sense that the response function can only be determined directly for elastic scattering and simplifying assumptions are required when applying it to inelastic scattering, increasing the experimental uncertainty, particularly very near the threshold. The procedure is not applicable below 10°, where elastic scattering cannot be measured, but reasonable assumptions are possible there. It appears safe to use the resonant vibrational excitation in N_2 as a secondary standard in the future, particularly in the forward direction.

The cross sections measured here agree well with many previous results, particularly the more recent measurements of Sun *et al* [5]. The agreement with existing data is generally better at intermediate angles, about 40–120°, and less satisfactory at smaller and larger angles. In particular, the present data at large angles are somewhat lower than those of Shyn and Carignan [34] and larger than those of Zubek *et al* 2000 [8]. A good agreement is also found with the majority of swarm and beam determinations of the integral and momentum-transfer cross sections.

Acknowledgments

I thank Hao Feng and Weiguo Sun (Sichuan University, People's Republic of China) and Michael A Morrison (University of Oklahoma, USA) for a private communication of their theoretical results. I further thank Michael A Morrison and Stephen J Buckman for helpful comments. This research is part of project no 200020-105226/1 of the Swiss National Science Foundation.

References

[1] Schulz G J 1973 *Rev. Mod. Phys.* **45** 423
[2] Itikawa Y 1994 *Adv. At. Mol. Opt. Phys.* **33** 253
[3] Zecca A, Karwasz G P and Brusa R S 1996 *Riv. Nuovo Cimento* **19** 1
[4] Brunger M J and Buckman S J 2002 *Phys. Rep.* **357** 215
[5] Sun W, Morrison M A, Isaacs W A, Trail W K, Alle D T, Gulley R J, Brennan M J and Buckman S J 1995 *Phys. Rev.* A **52** 1229
[6] Buckman S J and Brunger M J 1997 *Aust. J. Phys.* **50** 483
[7] Robertson A G, Elford M T, Crompton R W, Morrison M A, Sun W and Trail W K 1997 *Aust. J. Phys.* **50** 441
[8] Zubek M, Mielewska B and King G C 2000 *J. Phys. B: At. Mol. Opt. Phys.* **33** L527
[9] Trantham K W, Dedman C J, Gibson J C and Buckman S J 1998 *Bull. Am. Phys. Soc.* **42** 1727
[10] Read F H and Channing J M 1996 *Rev. Sci. Instrum.* **67** 2372
[11] Zubek M, Gulley N, King G C and Read F H 1996 *J. Phys. B: At. Mol. Opt. Phys.* **29** L239
[12] Cho H, Park Y S, Tanaka H and Buckman S J 2004 *J. Phys. B: At. Mol. Opt. Phys.* **37** 625
[13] Allan M 2001 *Phys. Rev. Lett.* **87** 033201
[14] Allan M 1992 *J. Phys. B: At. Mol. Opt. Phys.* **25** 1559
[15] Allan M 1995 *J. Phys. B: At. Mol. Opt. Phys.* **28** 5163
[16] Gopalan A, Bömmels J, Götte S, Landwehr A, Franz K, Ruf M W, Hotop H and Bartschat K 2003 *Eur. Phys. J.* D **22** 17
[17] Brunt J N H, King G C and Read F 1977 *J. Phys. B: At. Mol. Phys.* **10** 1289
[18] Allan M 2000 *J. Phys. B: At. Mol. Opt. Phys.* **33** L215
[19] Allan M 2004 *Phys. Scr.* T **110** 161
[20] Nesbet R K 1979 *Phys. Rev.* A **20** 58
[21] Read F H 1975 *J. Phys. B: At. Mol. Phys.* **8** 1034

[22] Read F H and Bowring N J 2005 The CPO-3D program www.electronoptics.com
[23] Pichou F, Huetz A, Joyez G and Landau M 1978 *J. Phys. B: At. Mol. Phys.* **11** 3683
[24] Brunger M J, Teubner P J O, Weigold A M and Buckman S J 1989 *J. Phys. B: At. Mol. Opt. Phys.* **22** 1443
[25] Asmis K R and Allan M 1997 *J. Phys. B: At. Mol. Opt. Phys.* **30** L167
[26] Allan M 2002 *J. Phys. B: At. Mol. Opt. Phys.* **35** L387
[27] Read F H 1968 *J. Phys. B: At. Mol. Phys.* **1** 893
[28] Nickel J C, Mott C, Kanik I and McCollum D C 1988 *J. Phys. B: At. Mol. Opt. Phys.* **21** 1867
[29] Shi X, Stephen T M and Burrow P D 1993 *J. Phys. B: At. Mol. Opt. Phys.* **26** 121
[30] Sohn W, Kochen K-H, Scheuerlein K-M, Jung K and Ehrhardt H 1986 *J. Phys. B: At. Mol. Phys.* **19** 4017
[31] Feng H, Sun W and Morrison M A 2003 *Phys. Rev.* A **68** 062709
[32] Feng H, Sun W and Morrison M A 2005 private communication
[33] Morrison M A and Trail W K 1993 *Phys. Rev.* A **48** 2874
[34] Shyn T W and Carignan G R 1980 *Phys. Rev.* A **22** 923
[35] Srivastava S K, Chutjian A and Trajmar S 1976 *J. Chem. Phys.* **64** 1340
[36] Brennan M J, Alle D T, Euripides P, Buckman S J and Brunger M J 1992 *J. Phys. B: At. Mol. Opt. Phys.* **25** 2669
[37] Sweeney C J and Shyn T W 1997 *Phys. Rev.* A **56** 1348
[38] Tanaka H, Yamamoto T and Okada T 1981 *J. Phys. B: At. Mol. Phys.* **14** 2081
[39] Jung K, Antoni T, Müller R, Kochem K H and Ehrhardt H 1982 *J. Phys. B: At. Mol. Phys.* **15** 3535
[40] Haddad G N 1984 *Aust. J. Phys.* **37** 487
[41] Phelps A V and Pitchford L C 1985 *JILA Information Centre Report* no 26, p 1
[42] Ramanan G and Freeman G R 1990 *J. Chem. Phys.* **93** 3120